

GLOBAL JOURNAL OF ENGINEERING SCIENCE AND RESEARCHES

EFFECT OF Ce DOPED ON THE STRUCTURAL, OPTICAL, ELECTRICAL AND SENSING PROPERTIES OF V₂O₅ THIN FILMS PREPARED BY CHEMICAL SPRAY PYROLYSIS

I.k.jassim^{*1}, Jamal. M. Rzaij², Iftikhar M. Ali³ and Isam M. Ibrahim³

^{*1}Professor, Department of physics, College of education, Tikrit University, Iraq

²Ph.D. student, Department of physics, College of science, Al Anbar University, Iraq

³Assistant Professor, Department of physics, College of science, Baghdad University, Iraq

ABSTRACT

V₂O₅ films doped with different cerium concentrations are deposited onto glass, p-type Si (111) and porous silicon (PS) substrates with temperature of 250 C by chemical spray pyrolysis technique (CSPT). V₂O₅ powder was dissolved in distilled water to prepare 0.05 M precursor solution. Ce doped vanadium oxide films were prepared, adding cerium oxide (CeO₂) with the ratios of 0%, 3%, 5%, 7% and 9% in separate solution. XRD analysis revealed a polycrystalline nature of the orthorhombic structure with the preferred orientation of (010) with nano crystallite size. Atomic Force Microscope (AFM) showed a good uniformity revealing a uniform growth of the films. The spectral absorption of the films occurred at the absorption edge of 550 nm. Un-doped V₂O₅ and doped with different concentration of Ce films have direct allowed transition band gap ranging from 2.2 eV to 2.55 eV according to dopant ratios of Ce. Electrical conductivity and Hall effect was studied to determine the type of prepared films. Sensitivity of NO₂ and H₂ gas at different doping ratios and different temperatures was calculated.

Keywords- vanadium oxide; thin films; structural properties; gas sensor.

I. INTRODUCTION

Thin films of semi-conducting materials generally have neither the same physical properties nor the same chemistry as the respective bulk material. Moreover, the preparing techniques and deposition processes used to create films dramatically change the physical properties of material such as refractive index, extinction coefficient, homogeneity, density, hardness, internal stress, adhesion to substrate and crystal structure. Therefore, the difference in physical properties between bulk and thin film material depends strongly on many factors such as the type of deposition process itself, deposition temperature, deposition rate, gas pressure, substrate geometry and preparation of the coating material and the post-deposition temperature [1].

Among the transition metal oxide semiconductors, vanadium pentoxide has drawn significant interest over the past decades owing to its wide range of applications . Its multivalency, layered structure, wide optical band gap, good chemical and thermal stability, excellent thermoelectric property, etc., are the characteristics that make vanadium pentoxide (V₂O₅) a promising material for applications in microelectronics , and for electrochemical and optoelectronic devices. It can be used as a catalyst, gas sensors , a window for solar cell and electrochromic devices as well as electronic and optical switches [2].

V₂O₅ is the most stable oxide and show semiconductor property with an energy gap of ~2.2 eV at room temperature [3], and displays electrochromic properties with varying color from blue to green and yellow within two seconds upon charging/discharging. Electrochromic materials change their optical properties reversibly during electrochemical reactions. These materials are used for smart windows, display devices and controlled reflectance mirrors [4].

Different literature reviews were added to study the structural, optical and electrical properties of Vanadium pentoxide thin films. Structure and semiconducting properties of amorphous vanadium pentoxide obtained by splat cooling [5]. Structural and optical studies for V₂O₅ thin films. The films gave two-step electrochromism, yellow to green and then green to blue [2]. Amorphous and crystalline of V₂O₅ thin films growled onto glass substrates with different concentrations from 0.1M to 0.5M Optical analyses showed the absorption coefficient shifts towards lower energies [6]. Developed a method of a facile synthesis for preparing nano-sized of V₂O₅ for high-rate lithium batteries using vanadyl oxalate in air [7]. In the present paper, un-doped vanadium pentoxide and doped with Ce thin films have been prepared by (CSPT) to produce large area and uniform coating [8].

II. EXPERIMENTAL PROCEDURE

Before starting the deposition, the solutions according to the films components was mixed then put it on the magnetic stirrer for about 15 minutes to be sure that the mixture solutions are mixed properly and to get solution with molarity of 0.05. Prior to deposition, Si substrates (for studying the structural properties) and PS (for studying the gas sensing properties) and glass substrates (for studying the optical and electrical properties) were cleaned and places on the flat plate heater surface, which it is an electrically controlled, and leaves them for about 10 minutes so as to allow their temperature to reach the set temperature at $(250 \pm 5) ^\circ\text{C}$. After that, can start the deposition process within deposition time of 5 sec. then stop this process for 10 sec. In the spray system, compressed and purified air was used as the carrier gas with a 3 kg/cm² pressure and the solution spray rate was maintained at 3 mL/min. The distance between the spray nozzle and the substrate was fixed at 30 cm. After the spray process is completed, then the hot plate will be shut down and the samples are left on the surface of the heater to reach the room temperatures, then the substrates can be raised. The X-ray diffraction (XRD) spectra of the films were obtained to verify their crystal structure using a (Cu-K α) radiation with $\lambda = 0.154$ nm. Optical transmission data were obtained using an UV-Vis double beam spectrometer at wavelengths ranging from 200 nm to 900 nm. Atomic force microscopy (AFM) was employed to observe the surface morphology of the films.

III. RESULTS AND DISCUSSION

1- Structural Properties

XRD patterns of un-doped V₂O₅ and doped with Ce are shown in **Figure (1)**. The films are polycrystalline with planes (200), (010), (110), (101), (400), (301), (600) and (002) which in agreement with [6][9]. The films are crystallized in orthorhombic phase according to International Centre for Diffraction (ICDPDF No.96-101-1226), which in agreement with [10][11][12][13], and with preferred orientation in the (100) direction at diffraction angle of $2\theta = 20.36^\circ$, $d = 4.35$ nm and lattice-parameter values of $a=11.4734\text{\AA}$, $b=4.35809\text{\AA}$ and $c=3.5533\text{\AA}$. It is very close to the result obtained in [11][14].

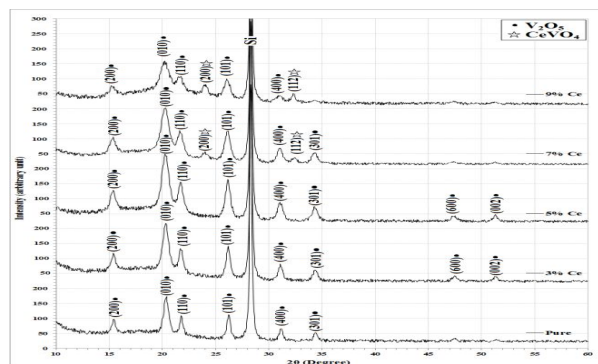


Figure (1): The XRD pattern of Ce doped V₂O₅ thin films.

The average crystallite size was calculated using Debye- Scherer's formula and it is found equal to 26.29 nm. For doping with cerium at the concentration of (3 and 5) %. there is no Ce containing phases were detectable, thus indicating a high dispersion of Ce or a very small crystallite size at these concentrations, which is the same result with [15]. When the doping was increased to 7%, two peaks with a weak intensity at about 2θ equal to: 24.01° and 32.4° for the planes (200) and (112) with tetragonal structure phase, characteristic of cerium orthovanadate (CeVO₄), according to the (ICDPDF NO.96-900-9764), which indicates that the effect of doping has led to the formation of new phase structure in V₂O₅ films and the atoms of doped material have successfully entered into the Vanadium oxide host lattice. [16].

When the doping rate reaches to the concentration of 9%, new phase of cerium orthovanadate (CeVO₄) will characteristic with a higher intensity for the new crystalline peaks comparatively with the dopant ratio of 7%, were observable at $2\theta = 24.03^\circ$ and 32.32° with a tetragonal structure for the planes (200) and (112), respectively, characteristic of (CeVO₄), according to the same card.

The average crystallite size (D_{ave}) for un-doped V_2O_5 and doped with CeO_2 was calculated by scherer and Williamson–Hall formulas, there was a small different in the value of (D_{ave}) between the two formulas, as listed in table (1).

Table 1. Crystallite size and strain of un-doped V_2O_5 films and doped with Ce; $D_{ave}(Sh)$ and $D_{ave}(W)$ are crystallite size extracted from scherer and Williamson-Hall relation respectively.

Doping Ratio	$D_{ave}(Sh)$ nm	$D_{ave}(W)$ nm	Strain
0%	26.29	20.69	0.0015
3%	23.31	19.26	0.0011
5%	17.82	14.75	0.0014
7%	17.52	14.29	0.0018
9%	15.84	9.43	0.0060

The variation of average crystallite size as a function of the doping ratio is shown in Figure (2), there was decrease in the D_{ave} value with increase of the dopant concentration at both methods which indicate to nanoparticles formed which it was resulting for the doping process, agreement with [10].

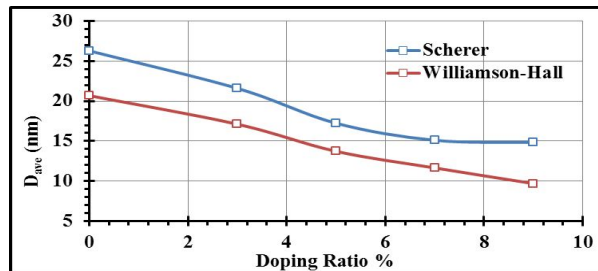


Figure 2. Crystallite size with doping ratio of un-doped V_2O_5 films and doped with Ce.

Table (2) shows the lattice constants (a, b, and c) of the V_2O_5 un-doped and doped with different concentration of Ce films. They are calculated by using the crystalline planes (200), (010) and (101), they were founded an increasing in lattice constants with increasing of the dopant concentration.

Table 2. Lattice constant for pure and doped films with Ce.

L.C Ce %	a (Å) EXP.	$\Delta a/a^\circ$	b (Å) EXP.	$\Delta b/b^\circ$	c (Å) EXP.	$\Delta c/c^\circ$
0	11.473	0.00061	4.358	0.000459	3.553	0.000563
3	11.503	0.002003	4.366	0.001376	3.558	0.000844
5	11.527	0.004094	4.373	0.002982	3.562	0.001969
7	11.551	0.006185	4.38	0.004587	3.566	0.003094
9	11.575	0.008275	4.387	0.006193	3.57	0.004219

Figure 2. Crystallite size with doping ratio of un-doped V_2O_5

Atomic Force Microscopy (AFM) Analysis

Figure (4-11) shows the Atomic force microscopy images and the chart of grain density distribution for V_2O_5 at different CeO_2 as doping rate of (0, 3%, 5%, 7% and 9%). which is deposited on glass substrate .AFM parameters contain average diameter, average roughness, average r.m.s roughness and peak –peak f value for these samples have been shown in table (3) which is illustrates decrement in average diameter with increasing of doping ratio from

0 to 9%, while the doped film by 5% Ce have maximum values of roughness and average r.m.s roughness value, (1.59nm) and (1.98), respectively.

Figure 3. AFM images and Size distributions for V_2O_5 at different doping ratios of Ce.

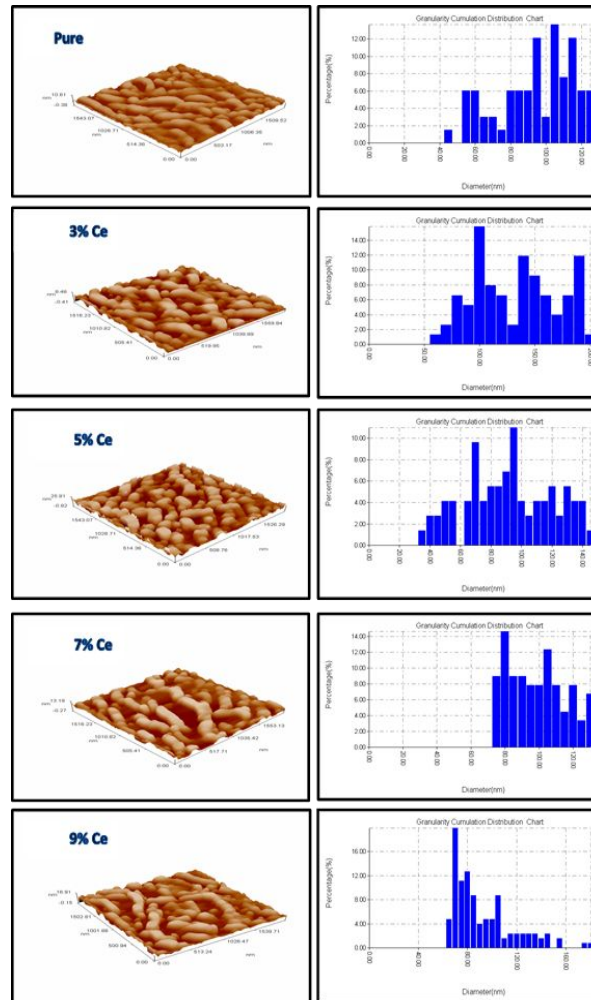


Figure 3. AFM images and Size distributions for V_2O_5 at different doping ratios of Ce.

Optical Properties

1- Transmission

Figure (4) shows the variation of transmittance as a function to the wavelength ranging from 300-900 nm. There was increasing in the transmittance spectrum with increasing of Ce dopant ratio. Transmittance increasing with strongly at the wavelength range of (300-550) nm, then stability after the absorbance edge. Rapid increasing in the transmittance within the range (300-550) nm and the relative stability within the range (550-900)nm, may be due to the electrons intraband transitions.

Un-doped V_2O_5 films and doped with Ce show a high transparency in the visible region. This is due to the lower film absorption [6], which means that films suitable as a window gap for solar cells because the effective spectral region in solar cells are located in the visible region of the spectrum.

The average transmittance at the range of (71-86)% for wavelengths longer than 564nm. Blue shifts towards lower wavelengths with increasing Ce concentration. The minimum value of transmittance is about (79%) which return to the Un-doped sample at 870nm wavelength rang, while the maximum value of transmittance is about (92%) which returns to the dopant sample with 9% Ce at 873 nm wavelength range.

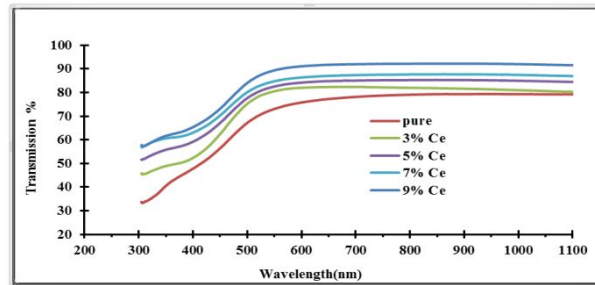


Figure 4. Transmission as a Function of the wavelength for un-doped V_2O_5 and doped with Ce at different doping ratio.

Table (4) show the maximum value of transmittance (T_{max})% of Un-doped and doped films, the value of transmittance at wavelength of absorbance edge (T_{edg})% and the transmittance at the wavelength of 500 nm ($T_{=500\text{ nm}}$)%.

Table (4): (T_{max})%, (T_{edg})% and ($T_{=500\text{ nm}}$)% of un-doped and doped V_2O_5 with Ce films as a function to the wavelength

Symbol	T_{max} %	$\lambda(T_{max})$ nm	T_{edg} %	$\lambda(T_{edg})$ nm	$T_{\lambda=500}$ nm %
pure	79	870	73	564	73
3%	82	687	81	551	81
5%	85	845	83	528	83
7%	88	874	85	506	85
9%	92	873	90	486	89

2- Optical Energy Gap (E_g)

Optical measurements can be used to estimate the energy difference between the valence and conduction bands, the optical band gap (E_g), which can help determine the electronic and thermoelectric properties of materials [17]. The optical energy gap values (E_g) have been determined by using Tauc formula, it is found that the relation for $r=1/2$ yields linear dependence, which means that the optical band gap has direct allowed transition. Extrapolating the straight line portion of the plot $(\alpha h\nu)^2$ versus $(h\nu)$ for zero absorption coefficient value gives the optical band gap (E_g). From Figure (5), we can observe that un-doped V_2O_5 and doped with Ce films have direct allowed transition band gap, it was founded about 2.2 eV. This result is reasonable and is very close to other (E_g) values found in literature [18][19] [20][21].

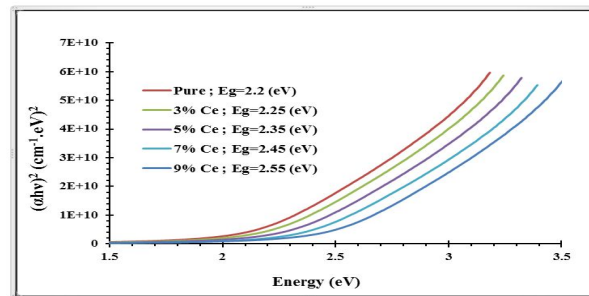


Figure (5): Tauc plot for un-doped V_2O_5 and doped with Ce at different concentrations.

The increasing of Ce concentration from 0 to 9% leads to increase the optical band gap from (2.2 to 2.55) eV, as shown in Figure (6), also there was shifting towards higher energies with increasing dopant concentration.

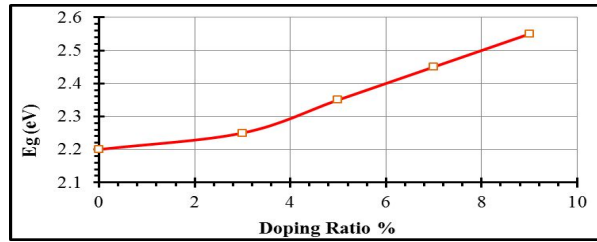


Figure (6): Variation of E_g with different doped concentration of Ce.

Electrical Properties

1. Resistance – Temperature Characteristic

Films were tested to confirm their semiconducting behavior. The sensor is placed on the heater and their resistances are measured in the range from (30 °C up to 200 °C), with step of 10 °C, in the dry air atmosphere. The films display high resistance at lower measuring temperature, and the resistance of the films decreased as the measuring temperature increasing as, seen in **Figure 7**. which is a semiconductor behavior.

1

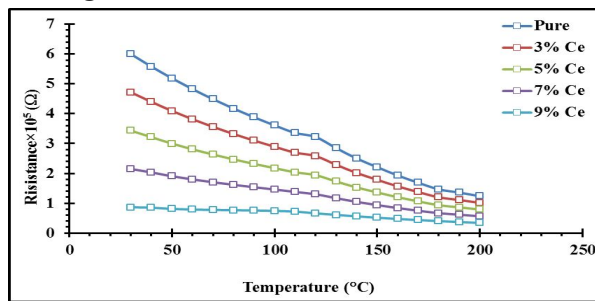


Fig.7 Resistance as a function to the temperature for un-doped V_2O_5 and doped with different ratio of Ce.

2. Hall Effect

The variation of carriers concentration (n_H) and Hall mobility (μ_H) of un-doped V_2O_5 and doped with Ce at different doping concentration thin films are shown in **table (5)**.

Table(5): Hall measurements of V_2O_5 thin films at different Ce dopant ratio.

Ce (%)	σ_{RT} ($\Omega^{-1}.cm^{-1}$)	R_H ($cm^3/coul$)	$n_H \times 10^{15}$ (cm^{-3})	Type	μ_H ($cm^2/v.s$)
0	0.1042	-7500	0.833	n	781.25
3	0.1325	-3500	1.786	n	463.83
5	0.1821	-1200	5.208	n	218.51
7	0.2909	-480	13.021	n	139.63
9	0.7228	-172	36.337	n	124.32

Hall measurements show that all films have a negative Hall coefficient which denotes to n-type charge carriers and the carrier concentration was increasing with the increasing of Ce dopant ratio, while there was a decrease in carrier mobility (μ_H) with increasing of Ce dopant concentration as shown in **Figure (8)**.

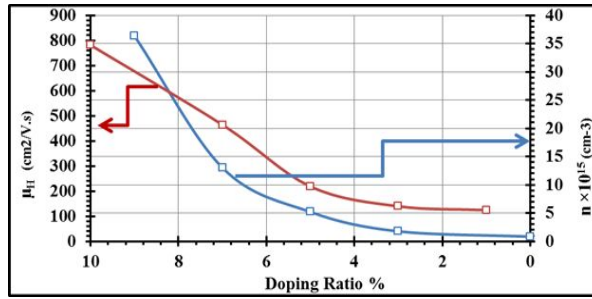


Figure 8. The variation of carrier concentration (n_H) and carrier mobility (μ_H) with different concentration of Ce doping ratio.

3. D.C conductivity

The variation of activation energy is summarized in table (6) and the plot of $\ln(\sigma)$ versus $10^3/T$ in the range of (303-473) K and temperature deposited at 250 °C on a glass substrate is shown in Figure (9).

Table 6. D.C activation energies, their ranges and conductivity at room temperature for thin V_2O_5 films at different Ce concentration

CeO ₂ (%)	E _{a1} (eV)	Temperature Range (K)	E _{a2} (eV)	Temperature Range (K)	σ_{RT} ($\Omega.cm$) ⁻¹
0	0.073	303-383	0.186	383-473	0.1042
3	0.070		0.182		0.1325
5	0.065		0.175		0.1821
7	0.055		0.163		0.2909
9	0.022		0.130		0.7228

It can be observed that two separated regions throughout the heating temperature range, the first region is at low temperature within the temperature range of (303-383)K and the second region is at higher temperature (383-473)K, indicating different conduction mechanisms dominating at specific temperature intervals. The activation energy in high temperature region was higher than that of low temperature region.

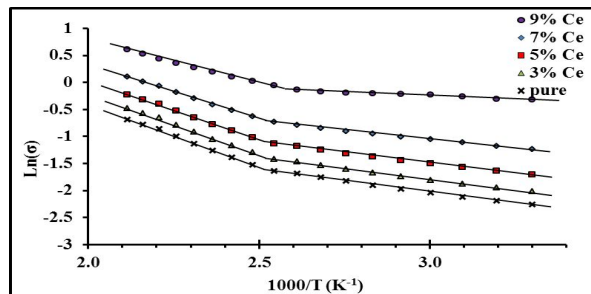


Fig.9 Plot of $\ln(\sigma)$ vs. $1000/T$ of un-doped V_2O_5 and doped with different ratio of Ce.

Figure (10) shows increasing of electrical conductivity with increase of doping concentration which resulting from the increase in the concentration of charge carriers because of the presence of donor levels in the energy gap. While there was decreasing in activation energy with increase of doping concentration at low temperature region.

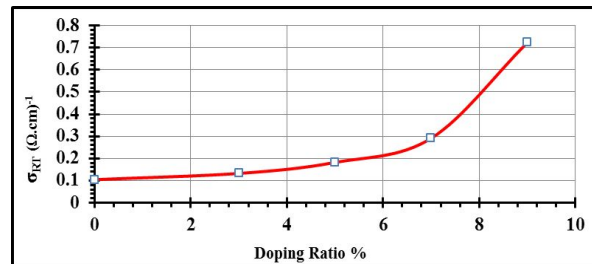


Fig.10 Variation of σ_{RT} with doping ratio for un-doped V_2O_5 and doped with different concentration of Ce doping ratio

Gas Sensing Measurement

1) Measurement of N₂ Gas

The thin films specimens are examined for gas sensing using NO₂ with concentration of 25 ppm at different operation temperature beginning from room temperature (30 °C) up to 200 °C with step of 50 °C. **Figure (11)** from **(a-e)** show the variation of resistance as a function of time with on/off gas valve.

The changing in conductivity essentially is due to the trapping of electrons at adsorbed molecules and band bending induced by these charged molecules. The negative charge (electrons) trapped in these oxygen species causes an upward band bending and thus a reduced conductivity compared to the flat band situation [22], when O₂ molecules are adsorbed on the surface of metal oxides, they would extract electrons from the conduction band E_c and trap the electrons at the surface in the form of ions. This will lead a band bending and an electron depleted region. For this reason we show from previous figures increasing in the resistance value when their films exposure to NO₂ gas.

The sensitivity factor (S%) at various operating temperatures is calculated using equation:

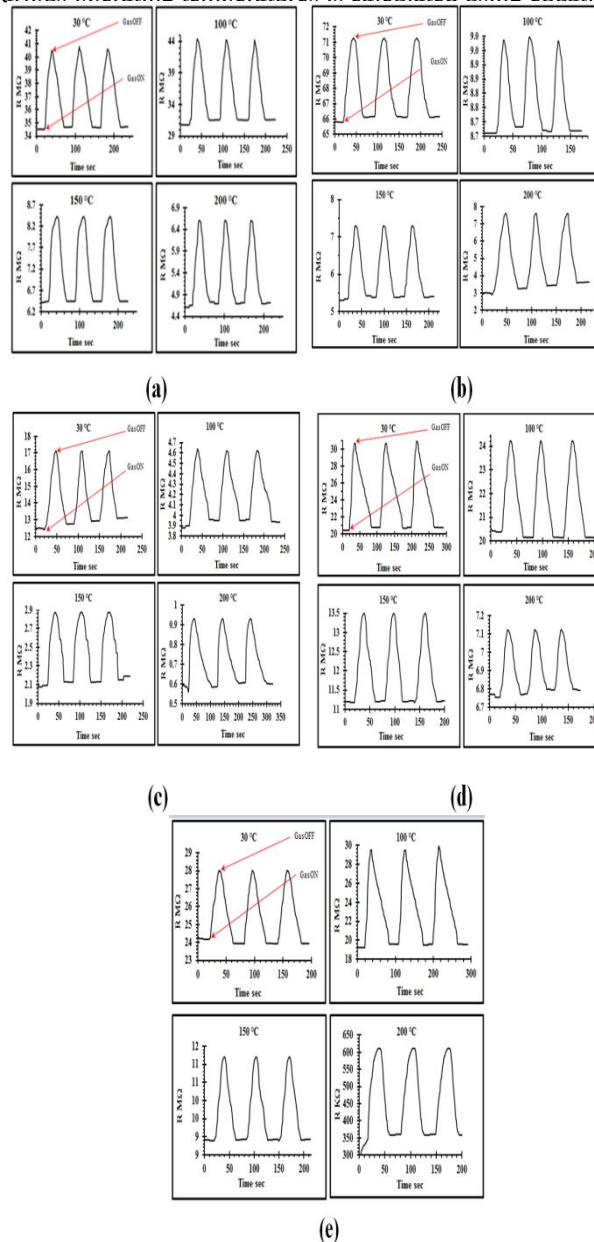


Fig. 11 The variation of resistance with time as NO₂ gas (a) Pure films, (b) 3%Ce, (c) 5% Ce, (d) 7% Ce and (e) 9% Ce.

where: is the sensitivity, and are the electrical resistance of the film in the air and electrical resistance of the film in the presence of gas, respectively.

Figure (12) shows the sensitivity as a function of operating temperature for un-doped V₂O₅ and doped with different concentration of Ce.

From Figure (12), The higher sensitivity may be return to the optimum number of inequality on the porosity, largest surface area, larger rate of oxidation and the optimum surface roughness.

The maximum sensitivity to NO₂ gas was observed to the film doped of 3% Ce and founded to be 150% at the optimal temperature (T₀= 200 °C), as shown in table (7).

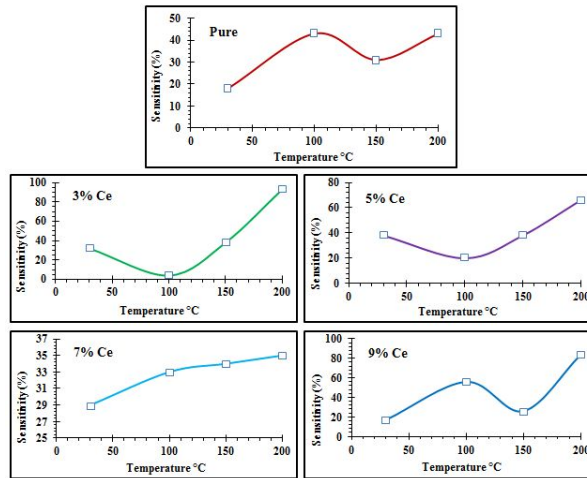


Fig.12 Variation of NO₂ sensitivity with operating temperature of un-doped V₂O₅ and doped with Ce thin films.

Table 7. Sensitivity% of un-doped V₂O₅ and doped with different ratio of Ce

Sample	Sensitivity % at			
	RT	100	150	200
pure	18	43	31	43
3%Ce	32	4	38	150
5% Ce	38	20	38	66
7% Ce	29	33	34	35
9% Ce	17	56	26	79

The relation between the response time and the Recovery time for gas with different Cerium Oxide doping ratio at optimum operating temperature of the un-doped and doped V₂O₅ thin films is shown in Figure (13).

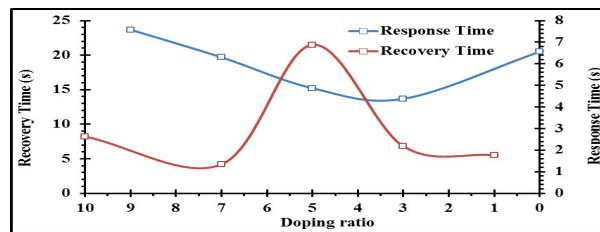


Figure 13. The variation of Response time and Recovery time for NO₂ gas with Ce doping ratio at optimum operating temperature T₀=200 °C.

The response speed is studied at the temperature at which the sensor exhibited a maximum sensitivity. The below figure shows that the 3% Ce doped samples at 200 °C exhibits a fast response speed (4.38 S) with recovery time (4.2 S) this revealed that a small quantity of impurities is **the best doping ratio** to achieve fast response sensor. The quick response sensor for NO₂ gas may be due to faster oxidation of gas, in addition, it can be attributed to the increasing in oxygen vacancies created upon V₂O₅:Ce lattice. Besides that, ions of Neodymium occupy energy level below conduction band and behave as an activator, consequently electrons easily move to conduction band, and increased the adsorption of oxygen on the surface extracts conduction electrons from the near surface region forming an electron depleted surface layer. That increased number of active adsorption sites and achieved fast response time for sensor's [23].

2) Measurement of H₂ Gas

The thin films specimens are examined for gas sensing using H₂ with concentration of 25 ppm at different operation temperature (100, 200 and 300) °C.

Figure (14) from (a-b) show the variation of resistance as a function of the time with on/off gas valve. There was decreasing in the resistance value when their films exposure to H₂ gas, (Gas ON), then the resistance value back downward at the closure of the gas (Gas OFF). The commonly accepted mechanism for that is based on the variation of the surface electron depletion region due to the reaction between hydrogen and the chemisorbed oxygen on the surface.

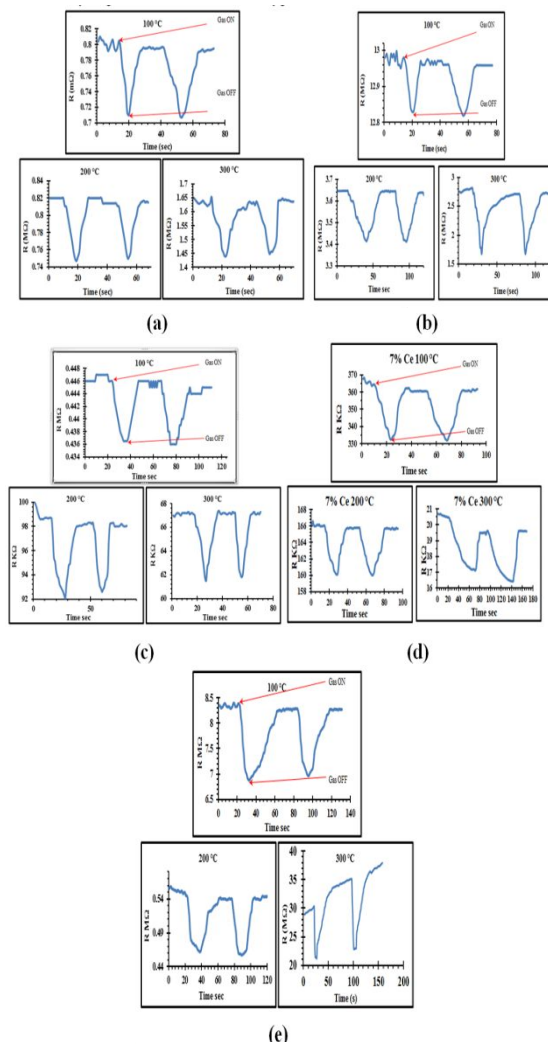


Fig.14 The variation of resistance with time as H₂ gas (a) Pure films, (b) 3%Ce, (c) 5% Ce, (d) 7% Ce and (e) 9% Ce.

Under an air atmosphere the oxygen molecules can get adsorbed on the surface of the semiconductor and extracts electrons from the conduction band to form oxygen ions. That may lead to the formation of an electron depletion region near the surface, which can greatly increase the resistance due to the decrease of net carrier density. When the sensor is exposed to a hydrogen atmosphere, the hydrogen molecules will react with the adsorbed oxygen species. The redox reaction is exothermic and results in the fast desorption of produced H₂O molecules from the surface. The released electrons will reduce the thickness of the depletion region, and decrease the resistance of the semiconductors. When the sensor is exposed to the air ambient again, the depletion region will be rebuilt by adsorbed oxygen species. The resistance will regain the initial level before hydrogen response. Moreover, the surface chemisorption of dissociated hydrogen may also play an important role in the hydrogen sensing behavior [24].

The sensitivity factor (S%) at various operating temperatures. The gas sensitivity tests performed at room temperature show no variation on the film conductivity, the **Figure (15)** shows the sensitivity as a function of operating temperature for un-doped V₂O₅ and doped with different concentration of CeO₂, which are deposited on the PS substrates. The gas sensitivity tests were performed at 100°C and increased to 300°C by 100 °C step.

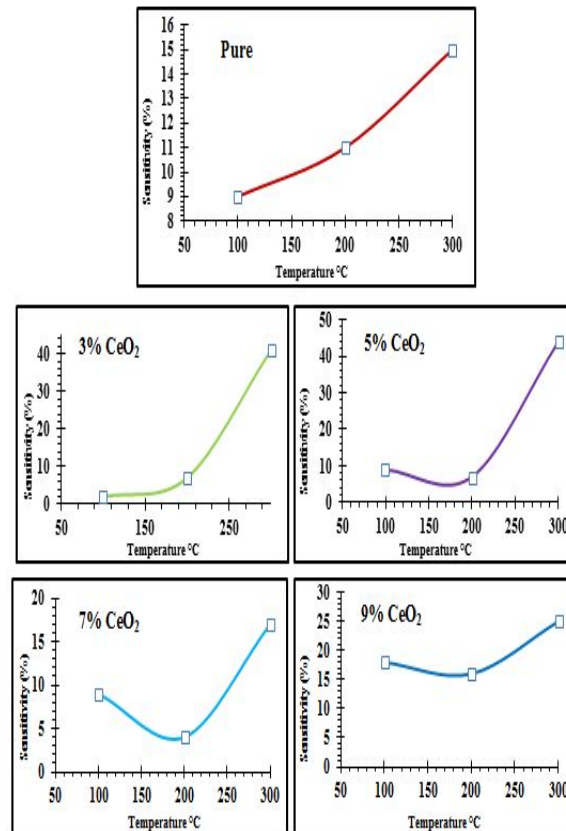


Figure (15): The variation of sensitivity with the operating temperature of the un-doped V₂O₅ and doped with Ce thin films.

Results show that the sensitivity of un-doped V₂O₅ and doped with ratio of 3% CeO₂ films increase with increasing of the operating temperature, which leads to an improvement of the films sensitivity may be is attributed to increase in the rate of surface reaction of the target gas. While the film doped with (5, 7, and 9)% with Ce there was decrease in sensitivity at the operating temperature of 200 °C and after this operating temperature the sensitivity return to increasing. The reason for this may be that the surface would be unable to oxidize the gas so intensively and the H₂ gas may burn before reaching the surface of the film at this temperature. Thus, the gas sensitivity decreases with increasing temperature. There was an increases and decrease in the sensitivity indicates the adsorption and desorption phenomenon of the gas. The higher sensitivity may be return to the optimum number of inequality on the porosity, largest surface area, larger rate of oxidation and the optimum surface roughness. The maximum sensitivity to H₂ gas was observed to the film doped 5% Ce and founded to be 44%, as shown in **table (8)**.

Table (8): Sensitivity% of un-doped V_2O_5 and doped with different ratio of Ce.

Sample	Sensitivity % at			
	RT	100	150	200
pure	---	12	9	12
3%Ce	---	2	7	41
5% Ce	---	9	7	44
7% Ce	---	9	4	17
9% Ce	---	18	16	25

The response speed is studied at the temperature at which the sensor exhibited a maximum sensitivity. **Figure (16)** shows that the 5% Ce doped samples exhibits a fast response speed (4.72) with recovery time (7.96 s) this revealed that a small quantity of impurities is **the best doping ratio** to achieve fast response sensor. While the slow response speed was observed for 3% Ce (9.91 s) with recovery time of (14.56 s).

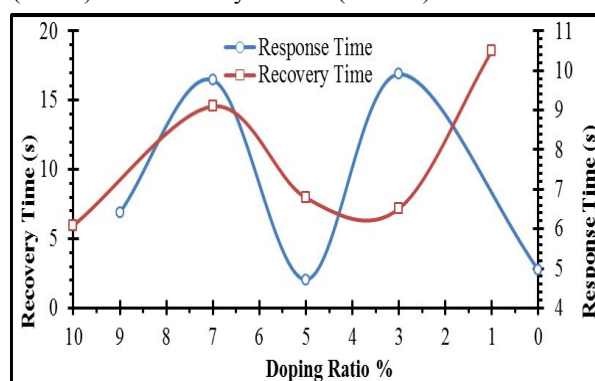


Figure (16): The variation of Response time and Recovery time for H_2 gas with Ce doping ratio at optimum operating temperature ($T_0=300\text{ }^\circ\text{C}$).

IV. CONCLUSION

In summary, pure Vanadium pentoxides and doped with 3%, 5%, 7% and 9% of Ce thin films were prepared using spray pyrolysis technique with 0.05 M on glass, Si and PS at substrate temperature of $250\text{ }^\circ\text{C}$. Structural analysis showed polycrystalline orthorhombic structure with (010) prefer orientation. When the doping was increased to 7% tetragonal structure phase characteristic of cerium orthovanadate ($CeVO_4$). Optical transmittance characteristic revealed increasing with increase doping ratio, also the direct allowed transition band gap increased with increasing of doping ratio. Electrical conductivity measurement showed two stages of conductivity throughout the heating temperature, first activation energy occurs at low temperatures while the second activation energy at high temperatures. Gas sensing measurement for NO_2 gas showed that **the best doping ratio** was 3% with sensitivity of 150% at $200\text{ }^\circ\text{C}$, while **the best doping ratio** was 5% with sensitivity of 44% for H_2 gas.

REFERENCE

- [1] M.C. Rao¹ and K. Ramachandra Rao², "Thermal Evaporated V_2O_5 Thin Films: Thermodynamic Properties," *Int. J. ChemTech Res.*, vol. 6, no. 7, pp. 931–3934, 2014.
- [2] M. Benmoussa, A. Outzourhit, A. Bennouna, and E. . Ameziane, "Electrochromism in sputtered V_2O_5 thin films: structural and optical studies," *Thin Solid Films*, vol. 405, no. 1–2, pp. 11–16, 2002.
- [3] C. W. Zou and W. Gao, "Fabrication , Optoelectronic and Photocatalytic Properties of Some Composite Oxide Nanostructures," vol. 11, no. 1, pp. 1–10, 2010.
- [4] K. Takahashi, Y. Wang, and G. Cao, "Growth and electrochromic properties of single-crystal V_2O_5 nanorod arrays," *Appl. Phys. Lett.*, vol. 86, no. 5, p. 53102, 2005.
- [5] L. RIVOALEN, A. REVCOLEVSCHI, J. LIVAGE, and R. COLLONGUES, "Amorphous vanadium pentoxide," *J. Non-Crystalline Solids*, vol. 21, no. 2, pp. 171–179, 1976.
- [6] M. A. Kaid, "Characterization of Electrochromic Vanadium Pentoxide Thin Films Prepared By Spray

- Pyrolysis," *Egypt. J. Solids*, vol. 29, no. 2, pp. 273–291, 2006.
- [7] A. Pan, J.-G. Zhang, Z. Nie, G. Cao, B. W. Arey, G. Li, S. Liang, and J. Liu, "Facile synthesized nanorod structured vanadium pentoxide for high-rate lithium batteries," *J. Mater. Chem.*, vol. 20, no. 41, p. 9193, 2010.
- [8] B. Thangaraju and P. Kaliannan, "Polycrystalline Lead Tin Chalcogenide Thin Film Grown by Spray Pyrolysis," *CRAT Cryst. Res. Technol.*, vol. 35, no. 1, pp. 71–75, 2000.
- [9] D. Johansson, "VO₂ films as active infrared shutters," *Ph.D.Thesis, University of LINKOPINGS*, P.67, 2011.
- [10] M. M. Margoni, K. Ramamurthi, S. Mathuri, T. Manimozhi, R. Rameshbabu, and K. Sethuraman, "Studies on Pure and Fluorine doped Vanadium Pentoxide Thin Films Deposited by Spray Pyrolysis Technique," vol. 7, no. 3, pp. 1072–1078, 2015.
- [11] a Chakrabarti, K. Hermann, and R. Druzinic, "Geometric and electronic structure of vanadium pentoxide: A density functional bulk and surface study," *Phys. Rev. B*, vol. 59, no. 16, pp. 583–590, 1999.
- [12] V. N. Shevchuk, Y. N. Usatenko, P. Y. Demchenko, O. T. Antonyak, and R. Y. Serkiz, "Nano- and micro-size V₂O₅ structures," vol. 4, pp. 67–71, 2011.
- [13] R. L. Josephine, S. Suja, and D. R. A, "Application of Renewable Energy Constant Current Source in The Formation of Uniform Surfaced," vol. 10, no. 8, pp. 3713–3716, 2015.
- [14] K. Hermann, M. Witko, R. Druzinic, A. Chakrabarti, B. Tepper, M. Elsner, A. Gorschlüter, H. Kühlenbeck, and H.-J. Freund, "Properties and identification of oxygen sites at the V₂O₅(010) surface: theoretical cluster studies and photoemission experiments," *J. Electron Spectros. Relat. Phenomena*, vol. 98–99, pp. 245–256, 1999.
- [15] "Supported Vanadium Oxide Catalaysts in Oxidation and Oxidative Dehydrogenation Reactions: Structure and Catalytic Properties," university of Pune, 2004.
- [16] J. Zhao, J. Ni, X. Zhao, and Y. Xiong, "Preparation and characterization of transparent conductive zinc doped tin oxide thin films prepared by radio-frequency magnetron sputtering," *J. Wuhan Univ. Technol.-Mat. Sci. Ed. J. Wuhan Univ. Technol. Sci. Ed. Mater. Sci. Ed.*, vol. 26, no. 3, pp. 388–392, 2011.
- [17] Z. M. Gibbs, A. LaLonde, and G. J. Snyder, "Optical band gap and the Burstein–Moss effect in iodine doped PbTe using diffuse reflectance infrared Fourier transform spectroscopy," *New J. Phys.*, vol. 15, no. 7, p. 075020, 2013.
- [18] Y. Vijayakumar, K. N. Reddy, and A. V. Moholkar, "Influence of the substrate temperature on the structural, optical and thermoelectric properties of sprayed V₂O₅ thin films," *Mater. Technol.*, vol. 49, no. 3, pp. 371–376, 2015.
- [19] N. M. Tashousha and O. Kasasbehb, "Optical Properties of Vanadium Pentoxide Thin Films Prepared by Thermal Evaporation Method," *JORDAN J. Pharm. Sci.*, vol. 6, no. 1, pp. 7–15, 2013.
- [20] L. A. R. L. P. A. J. C. Percino-picazo, "Photoluminescence in Nd-doped V₂O₅," *J Mater Sci*, vol. 5, no. 3, pp. 2298–2302, 2014.
- [21] M. Benmoussa, A. Outzourhit, R. Jourdani, and A. Bennouna, "Structural , Optical and Electrochromic Properties of Sol – Gel V₂O₅ Thin Films," *Act. Passiv. Elec. Comp.*, vol. 26, no. 4, pp. 245–256, 2003.
- [22] C. Wang, L. Yin, L. Zhang, D. Xiang, and R. Gao, "Metal Oxide Gas Sensors: Sensitivity and Influencing Factors," *Sensors*, vol. 10, no. 3, pp. 2088–2106, 2010.
- [23] T. Sujitno and S. Sudjatmoko, "The Influence of Platinum Dopant on the Characteristics of SnO₂Thin Film for Gas Sensor Application," *Atom Indo. Atom Indones.*, vol. 32, no. 2, 2011.
- [24] H. Gu, Z. Wang, and Y. Hu, "Hydrogen Gas Sensors Based on Semiconductor Oxide Nanostructures," *Sensors*, vol. 12, no. 5, p. 5517, 2012.